PIER C

(Received 29 November 2025, Accepted 26 January 2026, Scheduled 19 April 2026)

Small-Scale Fading Analysis under Human-Induced Blockage in Indoor Millimeter Wave Channels

Miguel Riobó Prieto, Manuel García Sánchez, and Iñigo Cuiñas*

AtlanTTic Research Center, Universidade de Vigo, Vigo, Spain

ABSTRACT: Millimeter-wave (mmWave) radio communication systems, essential to the advancement of future networks, are highly susceptible to link degradation caused by human body obstruction. This paper presents a comprehensive experimental study of fast fading phenomena induced by pedestrians crossing indoor mmWave links, specifically at 40 GHz and 60 GHz. The measurement campaign was conducted in a realistic access point to user equipment configuration, involving over 150 participants and yielding 604 fading events, of which 431 involved full line-of-sight (LOS) blockage. The analysis focuses on the statistical characterization of the deep-fade regions within these events. Results are compared with simulations based on the Knife-Edge Diffraction (KED) model to evaluate its accuracy under dynamic blockage conditions. The statistical analysis reveals that the Weibull distribution most effectively models the fast fading observed during human-induced blockage, outperforming Rician, Rayleigh, Nakagami-m, and Normal distributions — particularly at 60 GHz, where 89% of fades aligned with the Weibull model. Simulated fades using the KED model, however, did not show a strong fit with a single distribution yielding similar results to the Rician, Weibull, and Nakagami-m. These findings underscore the influence of diffracted multipath components in determining the statistical behavior of fast fading. The study confirms the limitations of existing diffraction models in capturing the full complexity of dynamic human blockage and highlights the need for refined modeling approaches. This work contributes critical insights toward the robust design and performance prediction of future indoor mmWave communication systems.

1. INTRODUCTION

Millimeter-wave (mmWave) frequency bands have become a key enabler for high-data-rate wireless communications, particularly in 5G systems operating in the upper segment of Frequency Range 2 (FR2) above 24 GHz and in local area networks, such as IEEE 802.11ad at 60 GHz [1]. These bands offer wide bandwidths, allowing for enhanced throughput, albeit with limited propagation range. This constraint can be beneficial in reducing interference and increasing frequency reuse, especially in indoor or enclosed environments where Device-to-Device (D2D) communications are prevalent. The global unlicensed status of the 60 GHz band further supports its practical deployment. However, millimeter-wave propagation faces several challenges, notably attenuation due to obstacles such as buildings [2–4], foliage [5], and particularly human bodies [6, 7], which can intermittently obstruct the Line-of-Sight (LOS) and cause significant degradation in link quality [8].

In response, various studies have sought to model human-induced fading effects at millimeter-wave frequencies. Theoretical analyses explore electromagnetic representations of the human body [9] and compare attenuation modeling approaches [10, 11]. Building on this approach, [12] proposed a simplified method for estimating the minimum diffraction loss and the average minimum diffraction by modeling three knife edges. However, the implementation reported in [10] indicates certain limitations, particularly in accurately reproducing the fine details of the fading phenomenon. Empirical investigations [7, 13–15] contribute with measurement-based models, while [16] examines fading depth, rise, and decay times in D-band measurements. Hybrid approaches combine electromagnetic modeling with measurements: for example, [17] applies the Double Knife-Edge Diffraction (DKED) model with a correction for the directional antennas used, [18] introduced a phase correction term to try to improve the fidelity of the model, and [19] uses flat-plate approximations with Universal Theory of Diffraction (UTD), both validated against real-world data. There are also more complex approximations using physical optics [20], which are effective but very computationally expensive. These works typically focus on large-scale fading parameters such as average attenuation, decay rates, and temporal characteristics [21], while often simplifying or excluding the analysis of rapid signal fluctuations during deep fades [22].

Despite recent progress in channel modeling, the behavior of fast fading nested within the troughs of human-induced large-scale fading remains poorly understood. Prior work such as [23] examined small-scale fading in open picocells, yet excluded the dynamic impact of moving individuals. Similarly, [24] addressed crowded cabin scenarios, but their analysis was restricted to static human obstructions. Finally, some studies like [25] did analyze the channel under dynamic conditions, but with the objective of integrated sensing, not channel characterization.

In contrast, this study targets the characterization of fast fading, specifically at the bottom of deep fades produced when

* Corresponding author: Iñigo Cuiñas (inhigo@uvigo.gal).

people block the line-of-sight in indoor radio links. Using a fast-sampling rate sounder in a realistic three-dimensional user equipment (UE) to access point (AP) communication scenario, the details of the fast-fading dynamics of the channel triggered by pedestrian-induced blockage can be captured and analyzed. Furthermore, by benchmarking the empirical results against KED model predictions, the aim was to highlight systematic discrepancies and evaluate the model's resilience under conditions where human-induced dynamics affect the propagation. In doing so, a more complete understanding of how fast fading manifests at the bottom of large-scale fades is provided, thereby contributing to the refinement of channel models for next-generation indoor wireless systems.

This paper is structured as follows. Section 2 summarizes the KED model. Section 3 describes measurement equipment and setup. Section 4 includes a brief overview of the measurement results and their processing. Section 5 compares the results of the simulations and measurements while Section 6 discusses the observations. Finally, Section 7 presents the conclusions.

2. KED MODEL

Human blockage in radio links has been widely characterized using KED models. A person is simulated by a vertical screen of infinite height but with a discrete width around which the signal is diffracted. For this study, we have considered a limited-height screen instead. The geometry of the problem is shown in Fig. 1, with the origin of the coordinate system on the transmitter (Tx) and the receiver (Rx) at an arbitrary point $\vec{r}$.

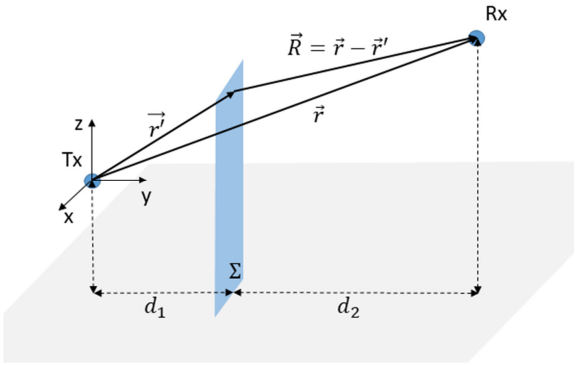

FIGURE 1. KED model geometry.

Let Σ be the screen, and d_1 and d_2 be the distances from the screen to the transmitter and receiver, respectively. The KED model can be expressed as the relationship between the scattered field around the screen, E_{sc}, and the free space field, E_{FS}.

$$\left.\frac{E_{sc}}{E_{FS}}\right|_{\theta} = 1 - \left[F\left(\nu_{x2}\right) - F\left(\nu_{x1}\right)\right]\left[F\left(\nu_{z2}\right) - F(\nu_{z1})\right] \quad (1)$$

In this equation, $F(v)$ is defined as:

$$F\left(\nu\right) = \frac{1+j}{2} I\left(\nu\right) \quad (2)$$

and it is dependent on the sine and cosine Fresnel integrals $S(\nu)$ and $C(\nu)$:

$$I\left(\nu\right) = C\left(\nu\right) - jS\left(\nu\right) \quad (3)$$

The parameters $\nu_{(x|z)}$ in (1) are the Fresnel-Kirchoff diffraction parameters and can be expressed as:

$$\nu_{x_{1|2}} = x'_{1|2}\sqrt{\frac{2}{\lambda}\frac{d_1+d_2}{d_1 d_2}} \quad (4)$$

$$\nu_{z_{1|2}} = \left(z'_{1|2} - \frac{d_1}{d_1+d_2}z\right)\sqrt{\frac{2}{\lambda}\frac{d_1+d_2}{d_1 d_2}} \quad (5)$$

where $x'_{1|2}$ and $z'_{1|2}$ are the horizontal and vertical limits of the screen, and $z = h_2 - h_1$ is the difference in antenna heights. If both antennas are at the same height ($z = 0$), then this solution is reduced to the KED formulation in [26].

3. MEASUREMENT SETUP

An experimental campaign was conducted to characterize human-induced fading on radio links at 40 GHz and 60 GHz, using two distinct geometries per frequency to ensure data diversity.

3.1. Measurement's Geometry

To emulate a typical AP-UE radio link, where the AP could be a router or a base station located on the side of a wall and the user equipment (UE) a mobile phone inside the pocket of the user, the AP antenna was positioned at 2.3 m above the floor and the UE at 0.88 m. Measurements were conducted in an open area at a corridor junction within the Telecommunications Engineering School (see Fig. 2), ensuring a clear line of sight (LOS) with no nearby obstructions. A rectangular grid was installed on the floor to guide participants along predefined perpendicular paths at known distances from the Tx. This layout facilitated an accurate analysis of human-induced fading as it facilitates the estimation of whether the user was obstructing the LOS. Furthermore, by selecting crossing points that induce LOS obstructions at different heights, the experiment incorporates diverse fading conditions. This methodological choice increases the statistical significance and generalizability of the results. Finally, the distances between the transmitter and receiver were chosen to maintain realistic conditions while ensuring that the received signal remained sufficiently above the noise level to be clearly

FIGURE 2. Measurement environment with reference grid on the floor. Tx antenna on the right, Rx on the left.

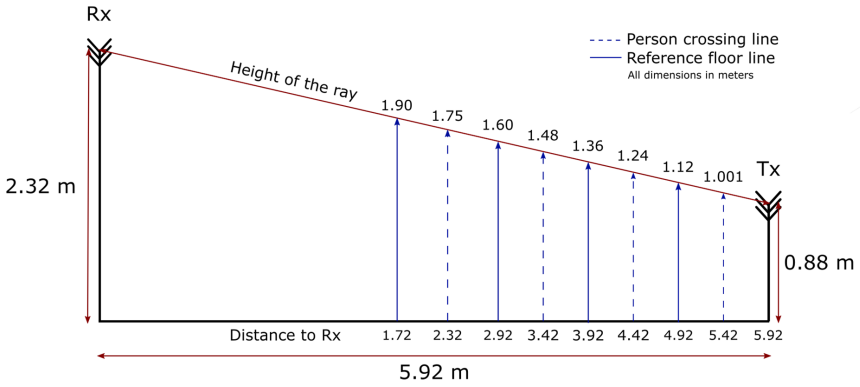

FIGURE 3. Example geometry of the 40 GHz experiment. Continuous lines represent the reference lines on the floor's rectangular grid. Discontinuous lines represent the crossing point for the individuals taking part in the experiment.

TABLE 1. Measurement setup at 40 GHz.

	Geometry 1	Geometry 2
Tx height (m)	0.88	0.85
Rx height (m)	2.32	2.3
Tx-Rx Distance (m)	5.92	6
Crossing points from Tx (m)	0.5, 1.5, 2.5, 3.6	1.24, 2.24, 3.24, 4.44

TABLE 2. Measurement setup at 60 GHz.

	Geometry 1	Geometry 2
Tx height (m)	0.8	0.7
Rx height (m)	2.26	2.1
Tx-Rx Distance (m)	4.84	4.83
Crossing points from Tx (m)	0.72, 1.72, 2.72, 3.82	0.6, 1.6, 2.6, 3.7

distinguishable. An example setup for 40 GHz (Geometry 1) is shown in Fig. 3, with full geometric details provided in Tables 1 and 2.

In the 40 GHz campaign, 61 individuals crossed the radio link at walking speed, while 90 participated in the 60 GHz campaign. Each volunteer crossed the link up to four times, resulting in 244 and 360 fading events, respectively. The difference in participant numbers reflects the voluntary nature of the study and its execution on different days. All participants were informed of the experiment's purpose and provided their consent.

The height distribution of the individuals that took place in the experiment is depicted in Fig. 4. The values range from 1.51 m to 1.95 m with an average value of 1.74 m. Given that the country's average height is 1.75 m for men and 1.63 m for women, the participants in this experiment lie on the taller side.

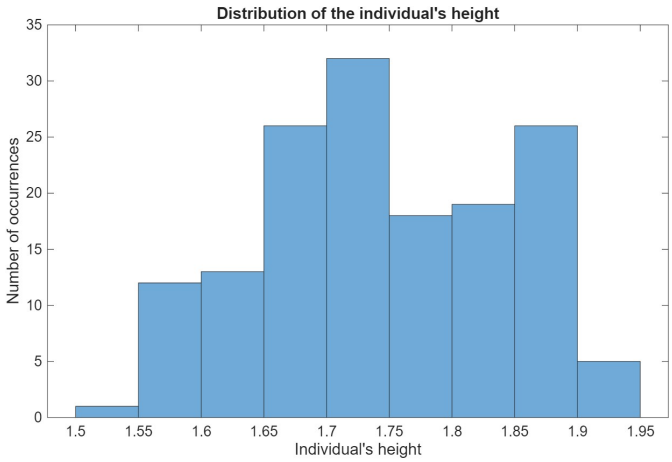

FIGURE 4. Distribution of the height of all the individuals that took part in the experiment.

3.2. M easurement Equipment

Data acquisi tion was automated using MATLAB to control a Rohde & Schwarz ZVA67 Vector Network Analyzer (VNA). A continuous single-tone signal was transmitted, and the S_{21} parameter was recorded. Transmission occurred from VNA port 1 via a power amplifier (35 dB gain at 40 GHz; 23 dB at 60 GHz) feeding an omnidirectional antenna (Flann Microwave MD249-AC at 40 GHz; MD249-AA at 60 GHz). The signal was received at the AP by a horn antenna (Flann Microwave 23240-20 at 40 GHz; QSH25F20 at 60 GHz) connected to port 2 of the VNA. In the 60 GHz setup, an additional 23 dB amplifier was placed between the receiving antenna and the VNA. Each measurement lasted 5 seconds, and the system was calibrated prior to the campaign.

4. FADING ANALYSIS AND KED SIMULATION

4.1. Experimental Observations

Figures 5 and 6 illustrate fading traces for the 40 and 60 GHz experiments. During clear line-of-sight (LOS) conditions (samples 0–2000 on the first image), the signal remains stable. As a person approaches the direct path (samples 2000–2700), signal variability increases, culminating in a pronounced attenuation when LOS is fully obstructed (samples 2700–3300). After the fading event, the signal gradually returns to a steady state. This ripple pattern, consistent with findings in [27] and similar to those in [11, 14, 21], is likely caused by diffraction effects as the person enters the first Fresnel zone. The variability of the

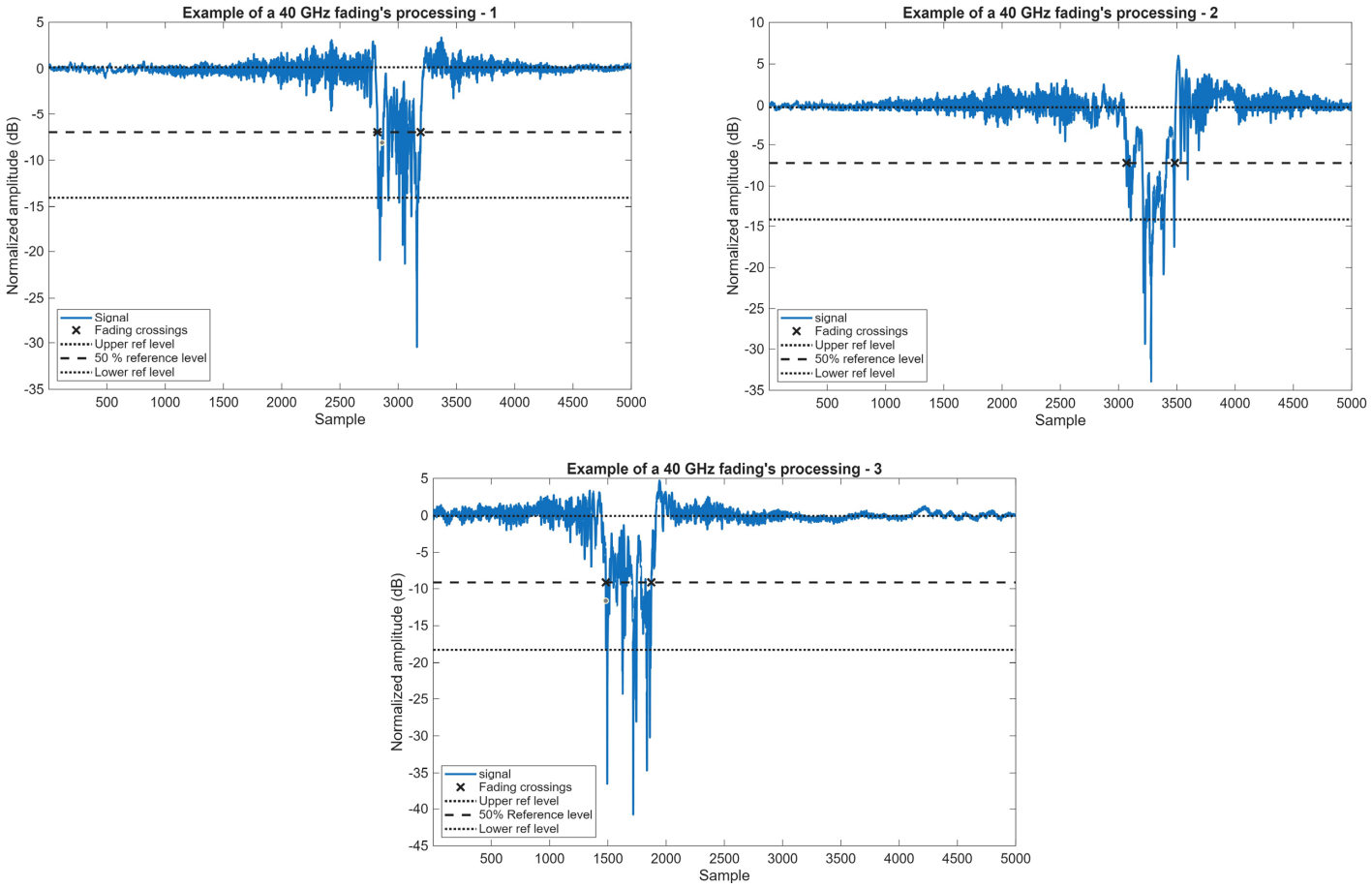

FIGURE 5. Examples of a measured 40 GHz fading event with the points used to define the fading overlayed.

deepest fade of the channel could be due to the combination (both constructive and destructive) of different diffracted rays. In some cases (like the second plot in Fig. 5), there is a more specific shape consisting of a first dip after the main one that could have been caused by a swinging arm that interrupts the LOS before the torso of the individual does it. Similar results were observed in the rest of the measurements.

4.2. KED Simulations

To simulate attenuation using the KED model, the parameters — such as antenna heights, individual height, and distances to the obstruction screen, denoted as $(d_1, d_2, h_{tx}, h_{rx}...)$ — were set to match the measurement setup, as detailed in Tables 1 and 2. Only two parameters required specification: the screen width, which was set to $w = 0.28$ m to avoid multiple simulation parameters and to keep it in line with what was used in [16] and [17]; and its discrete positions along the path, in 0.002 m increments, simulating a continuous walk across the link with partial and full LOS blockage.

Figure 7 presents the simulated fading caused by a 1.82 m tall individual crossing the link 5.42 m from the UE at 40 GHz, while Fig. 8 shows a simulation at 60 GHz of a 1.73 m tall person crossing the radio link at 4.12 m from the UE. Ripples appear both before and after the main fading event, as well as within the attenuation dip — features also observed in the measurements (Fig. 5, Fig. 6) — likely resulting from constructive and destructive interference due to phase variations of the diffracted components around the screen.

4.3. Data Processing

Fading segments were stored for subsequent analysis. Given the multi-day duration of the measurement campaign, and although the VNA was calibrated, small level drifts due to temperature and other environmental factors were corrected. Each trace was normalized to its LOS reference by estimating the signal level immediately prior to obstruction and shifting the trace accordingly. This normalization step improves the reliability of the statistical analysis.

To isolate fading events, only Non-Line-of-Sight (NLOS) signal traces were selected (those where the subject's height was sufficient to block the direct AP-UE path) resulting in 431 valid events (173 at 40 GHz and 258 at 60 GHz). Then, an edge-detection algorithm was applied to identify the ascending and descending flanks of each fading event. This algorithm relied on modeling the signal as a two-state process. Upper and lower levels were estimated using the histogram method described in [28], and the midpoint crossings were calculated. In Fig. 5 and Fig. 6, these levels are represented as dotted lines, while the 50% level is shown as a dashed line, with the midpoint crossings on the descending and ascending branches marked by

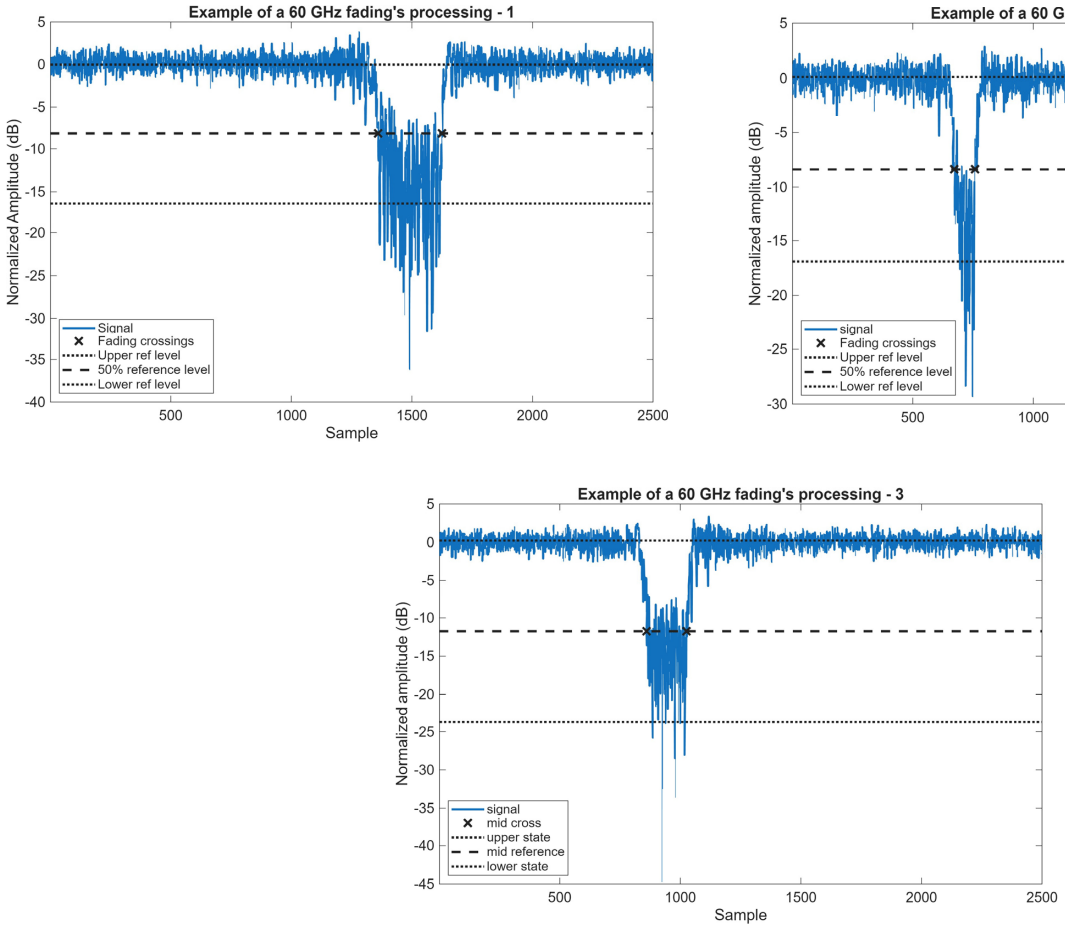

FIGURE 6. Examples of a measured 60 GHz fading event with the points used to define the fading overlayed.

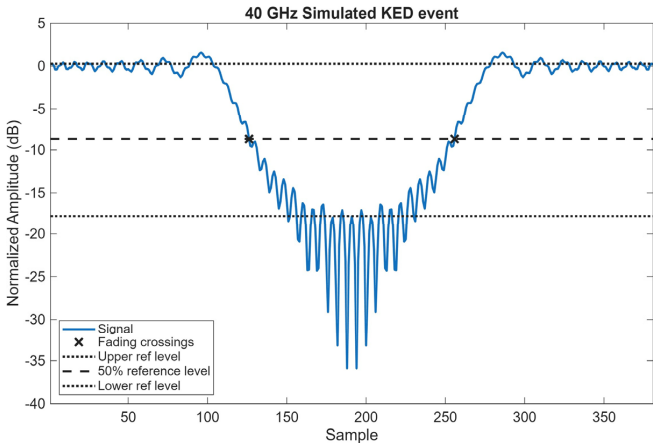

FIGURE 7. Example of a 40 GHz KED simulation fading event.

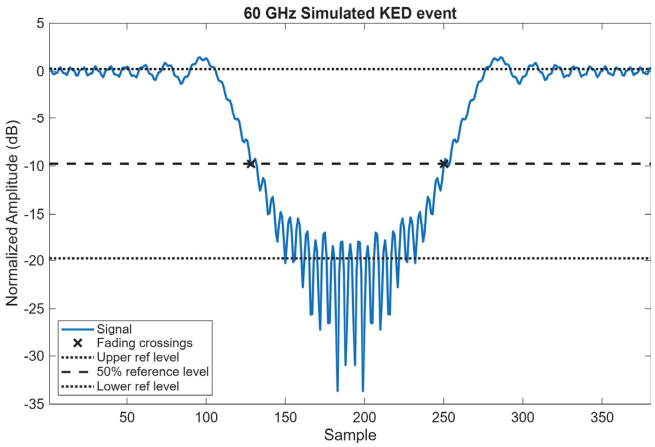

FIGURE 8. Example of a 60 GHz KED simulation fading event.

an "×" on this line. Samples between the first and last crossing points (marked "x") were classified as fading and analyzed to determine the best-fitting statistical distribution. The signal samples between these edges were normalized by their mean value in natural units (n.u.) and used for further analysis. Since the objective of this work is to study the variability of the signal level around the fading's mean value but not the mean value itself, it is necessary to normalize the fading level with respect to the average value of the fading to isolate this variability.

5. RESULTS

As is well known, the KED model does a fairly good job in approximating the maximum attenuation [17, 21, 23, 29], but it is less precise when modeling the variability of the fading. To better characterize the fast fading during LOS blockage events, several candidate distributions were considered, including Normal, Rician, Rayleigh Weibull, and Nakagami-m. The measured data together with simulated KED samples were subjected to a goodness-of-fit evaluation using the Chi-square and

TABLE 3. Distribution fitting results Alpha $= 0.05$.

	40 GHz				60 GHz			
	Meas.		Sim.		Meas.		Sim.	
Distribution	Chi-sq	KS	Chi-sq	KS	Chi-sq	KS	Chi-sq	KS
Normal	**21%**	59%	50%	68%	68%	91%	35%	76%
Rician	20%	65%	44%	**76%**	83%	93%	49%	87%
Rayleigh	14%	37%	**56%**	48%	71%	79%	**67%**	55%
Weibull	21%	**72%**	43%	**76%**	**89%**	**98%**	49%	**88%**
Nakagami-m	19%	65%	39%	**76%**	86%	97%	49%	**88%**

Kolmogorov-Smirnov (KS) tests, both at the 5% significance level (Table 3). This significance level was selected because it is a conventional threshold in statistical analysis that balances sensitivity to deviations with robustness against false positives. The number of bins was set to 10. Given that the fadings contained approximately 200 samples on average, there are about 20 samples per bin. However, a minimum of 5 samples per bin was set, meaning that if a bin has fewer than 5 samples, it would be merged to the adjacent one, thus increasing the number of samples in that bin. To complement this, the Kolmogorov-Smirnov statistic (KS Statistic) is also computed as a continuous measure of discrepancy between empirical and theoretical cumulative distributions (Table 4). The value reported in this paper is the average of the KS statistic of all the goodness-of-fit tests performed on all the available data. This dual approach ensures that the analysis captures not only whether a distribution can be formally accepted under conventional thresholds, but also the magnitude of deviation, offering a more complete assessment of the model's adequacy. In Tables 3 and 4, the best-fit results are highlighted in bold.

TABLE 4. KS-statistics results.

	40 GHz		60 GHz	
Distribution	Meas.	Sim.	Meas.	Sim.
Normal	0.10	0.11	0.09	0.10
Rician	0.10	**0.10**	0.08	**0.09**
Rayleigh	0.15	0.23	0.11	0.23
Weibull	**0.09**	**0.10**	**0.07**	**0.09**
Nakagami-m	0.10	0.11	0.08	**0.09**

5.1. 40 GHz

At 40 GHz, the Chi-square test indicated that 21% of the measurement sets were consistent with both the Normal distribution and the Weibull distribution, whereas the Kolmogorov-Smirnov test identified the Weibull distribution as the best candidate with 72% of samples passing the goodness of fit criteria. Moreover, the average KS statistic across all samples was the lowest for the Weibull, confirming its superior alignment with the empirical data. The reported percentages correspond to the proportion of measurement sets that passed the goodness-of-fit test under each threshold, providing a practical way to compare competing distributions across multiple realizations. Taken together, these complementary metrics consistently point to the Weibull distribution as the most suitable model for fast fading at this frequency.

To provide a model representative of the data, the parameters that characterize that $Weibull(\lambda, k)$ distribution scale (λ) and shape (k) were obtained using all the samples' sets (not only the ones that pass the goodness of fit criteria) and averaged out. The resultant distribution is a $Weibull(1.12, 2.69)$ with the following confidence intervals $\lambda = [1.11, 1.13]$, $k = [2.45, 2.93]$. Table 5 summarizes these results.

TABLE 5. Derived Weibull parameters. Confidence intervals inside brackets.

	40 GHz	60 GHz
Scale - λ	$1.12 \sim [1.11, 1.13]$	$1.12 \sim [1.11, 1.13]$
Shape - k	$2.69 \sim [2.45, 2.93]$	$2.20 \sim [2.07, 2.34]$

In contrast, the KED simulated samples yielded less conclusive results. Depending on the goodness-of-fit test used, the most suitable distribution varies. On the one hand, in the case of the Chi-square test, at a 56% acceptance most of the samples are consistent with a Rayleigh distribution. On the other hand, the KS test shows a tie among Rician, Weibull, and Nakagami with 76% of the samples classified as such. Regarding the KS statistics, the Nakagami lies slightly behind Rician and Weibull. Fig. 9 contains examples supporting these observations.

5.2. 60 GHz

Results at 60 GHz are more conclusive, with the Weibull distribution being consistent with 89% and 98% of the fading events when evaluating through Chi-square and KS, very closely followed in both cases by Nakagami-m and Rician distributions at 86% and 83%, respectively for the chi-square goodness-of-fit test and 97% and 93% for the KS. The KS statistic also points to Weibull as the one that has an average lower discrepancy between empirical and theoretical cumulative distributions with a value of 0.08. The estimated Weibull distribution parameters were $Weibull(1.12, 2.20)$ with confidence intervals of $\lambda = [1.11, 1.13]$, $k = [2.07, 2.34]$ (see also Table 5).

Regarding the KED-simulated data, the results are less clear than those obtained with the measured data. The Chi-Square

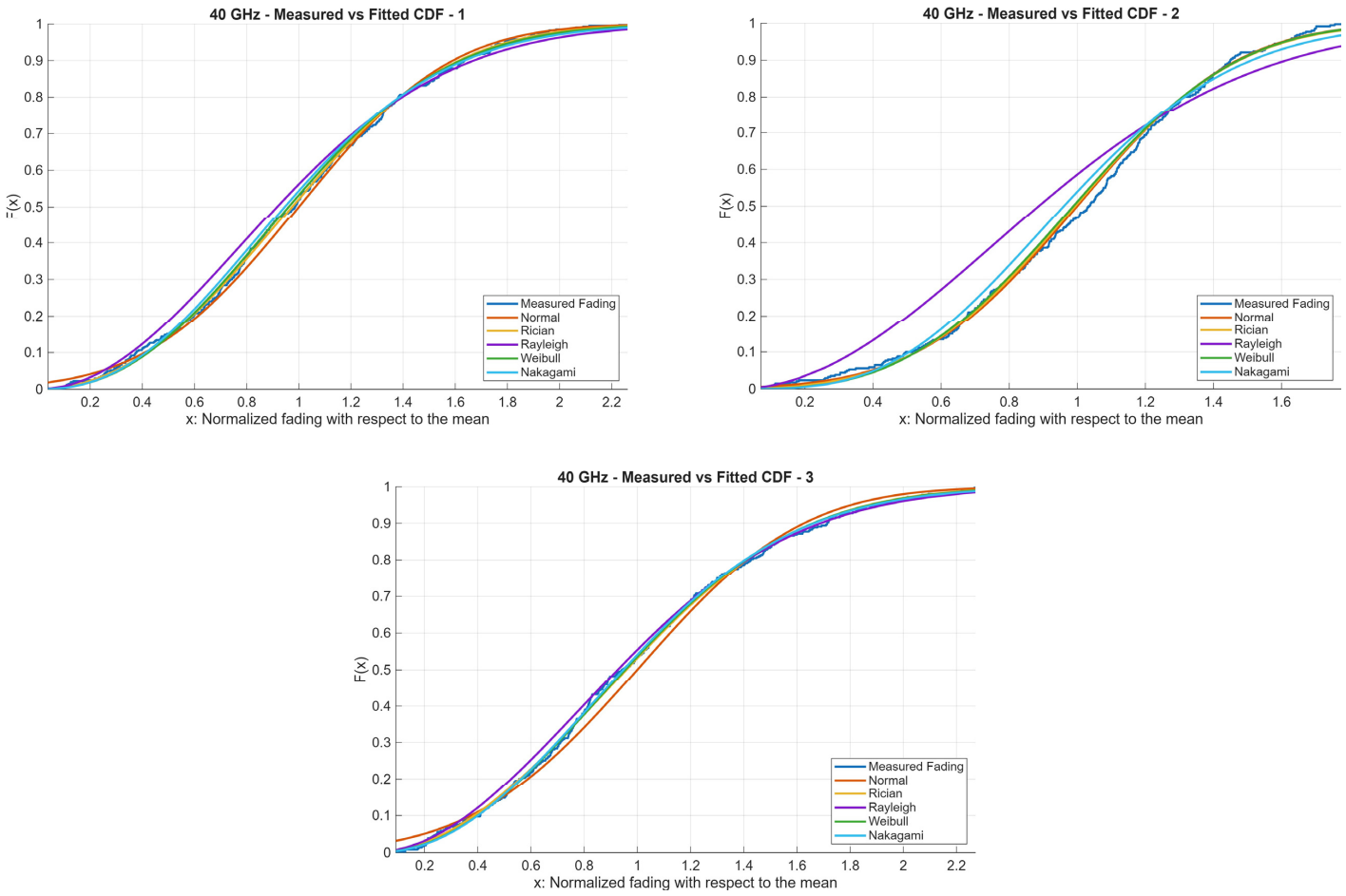

FIGURE 9. Examples of the CDF of three different sets of 40 GHz fadings and their fitted distributions.

TABLE 6. RMSE results.

	40 GHz		60 GHz	
Distribution	Meas.	Sim.	Meas.	Sim.
Normal	0.05	0.05	0.04	**0.04**
Rician	0.05	**0.04**	0.04	**0.04**
Rayleigh	0.08	0.11	0.05	0.11
Weibull	**0.04**	**0.04**	**0.03**	**0.04**
Nakagami-m	0.04	**0.04**	**0.03**	**0.04**

test continues to favor the Rayleigh distribution, with 67% of the datasets meeting the criterion. In contrast, the Kolmogorov-Smirnov test indicates that the Weibull and Nakagami distributions both satisfy 88% of the measurement sets, with the Rician distribution following closely at 87%. However, the KS statistic is unable to discriminate between Weibull and Nakagami, as both exhibit the same divergence of 0.09 between the empirical and theoretical cumulative distribution functions. An illustrative example of a measured fading cumulative distribution function (CDF) and different distributions adjustment is provided in Fig. 10.

Finally, the average root-mean-square error (RMSE) value among all empirical distributions and their corresponding theoretical value were also computed and presented in Table 6. Results obtained regarding the distribution with the lower RMSE match those of the distributions with the lower KS statistic, showing coherence between the two metrics. Furthermore, the resultant value is in order with those found in the literature [13, 14], reinforcing the soundness of the analysis. Best fits in Table 6 are indicated in bold.

6. ANALYSIS OF THE RESULTS

The results obtained align with previous literature. Studies such as [30] and [31] indicate that multipath fading tends to follow a Weibull distribution when the wave propagates through a nonhomogeneous environment, where the number of available propagation paths is limited, and the reflected or scattered components have unequal power levels. These conditions can be consistent with the scenario in which a human body obstructs the LOS path. Owing to the inherently nonhomogeneous structure of the human body — limbs in motion and irregular geometry, partially considered in [32] — the scattered and diffracted components around the person can exhibit different power levels and are relatively sparse. This combination of a small number of effective paths and unequal component powers can naturally lead to a Weibull distributed envelope, which aligns with the behavior observed in the measured data.

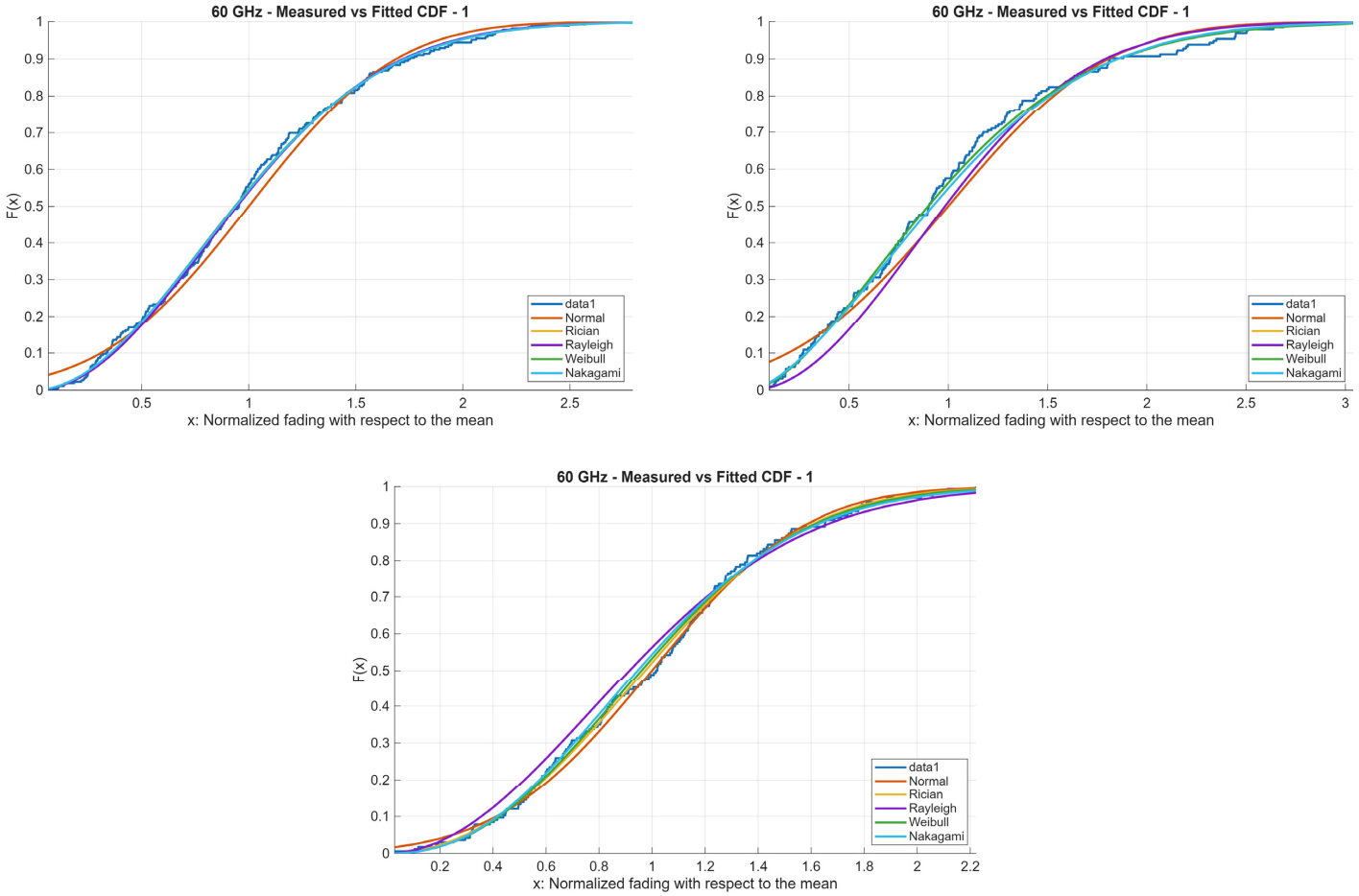

FIGURE 10. Examples of the CDF of three different sets of 60 GHz fadings and their fitted distributions.

Regarding why the Weibull distribution fits the results much better at 60 GHz than at 40 GHz, one plausible explanation is related to the propagation characteristics at these frequencies. At 40 GHz, the channel experiences lower attenuation and higher penetration through the person's torso, which creates a more complex environment with multiple interacting components. This complexity makes it difficult to model the behavior with a single distribution, as the observed data likely reflect a mixture of different propagation effects. In contrast, at 60 GHz the channel is dominated by fewer multipath components due to higher attenuation and reduced penetration, resulting in a simpler propagation scenario that can be effectively captured by a single distribution, such as Weibull. This reasoning aligns with the observation that, at 40 GHz, none of the tested statistical distributions fit the data well, while at 60 GHz, the match is much more evident. Nonetheless, further research would help confirm this hypothesis.

With respect to the KED simulated data, no clear conclusion can be drawn. The conditions required for Rician fading are well established: the presence of a line-of-sight or dominant component, multipath components with comparable average power, and a sufficiently large number of incoming waves [29]. Rayleigh fading is a particular case of the Rician, where there is no dominant LOS component, while Nakagami and Weibull are empirical models used to capture fading envelopes beyond the classical Rayleigh and Rician assumptions. It seems that for the simulations, none of those scenarios are particularly dominant, and thus, there is not a single distribution that is the better representation of the data. Therefore, although KED performs well in predicting the maximum attenuation produced, it fails when simulating the entire fading process. The amplitude distribution of the bottom of the fading does not seem to clearly match the Weibull distribution observed in the measurements. This is probably because of the more complex real scenario in which humans are not perfect screens, especially at higher frequencies. The movement of the arms can also have an influence, interrupting the LOS before the user and creating some phase variations that cannot be accounted for in the model.

These findings not only validate the relevance of the Weibull distribution in modelling fast fading under human-induced blockage but also expose the limitations of classical diffraction-based models, such as KED, when applied to dynamic indoor scenarios. The contrast between measured and KED-simulated data highlights the complexity of real-world propagation phenomena, especially in environments where human movement is frequent and unpredictable.

When comparing these results with the models presented in the introduction [10, 17, 21], the improvement of the fast fading characterization can be clearly stated. Most of these models do not characterize fast fading; in contrast, those that do

characterize it provide only a limited analysis of its distribution. We believe that the distribution derived in this paper can be combined with those existing models to generate a hybrid physical-statistical model in which the maximum attenuation and the shape of the fading can be modeled using any of the mentioned methods, and then, the variability at the bottom of the fading can be added using the Weibull distribution with the proper parameters depending on the frequency of operation.

The main limitation of this study is that it was only conducted at two frequencies, so it would be interesting to extend it to other bands like 28 GHz and 70 GHz to check the results.

An additional line of research would be to extend this study to wideband channels to evaluate their performance under similar conditions. Due to the bandwidth of the channel being larger than the coherence bandwidth, wideband channels inherently mitigate the effects of frequency-selective fading, as attenuation occurring at one frequency may not be present at another, which would result in a fading event with much less variability, as shown in [18]. Nevertheless, further research on this behavior would provide valuable insights into the robustness of the proposed approach.

7. CONCLUSIONS

This paper reports an extensive measurement campaign modeling the fading's trough in a realistic 3D indoor scenario representative of a typical AP-UE radio link. Conducted at 40 GHz and 60 GHz, the campaign involved 152 individuals of varying heights crossing the link at four different distances, yielding 604 fading events. Measurements were narrowband with high sampling rates, capturing fading events at fine temporal resolution. Of these, 431 events with complete LOS obstruction were analyzed. The fading was also simulated using the KED model for comparison.

Results summarized in Table 4 show that the Weibull distribution is the best fit for the measured fading events at both frequencies, having the lowest KS-statistic and accounting for 21% (Chi-Square) and 72% (Kolmogorov-Smirnov) at 40 GHz, and 89% (Chi-Square) and 98% (Kologorov-Smirnov) at 60 GHz of the fading events at the 5% significance level. Conversely, for the KED-simulated fading events, no clear candidate is deduced, as the results show agreement with Rician, Rayleigh, Weibull, and Nakagami distributions depending on the goodness-of-fit method used.

By addressing a previously unexplored aspect of fading — its behavior during complete LOS obstruction — this work contributes a novel and empirically grounded perspective to the field. The scale of the measurement campaign, the dual-frequency analysis, and the integration of theoretical modelling provide a robust foundation for future research. Ultimately, these insights are expected to inform the development of more accurate channel models and enhance the design of resilient mmWave communication systems in human-populated environments, based on, i.e., the proactive detection of blockage [33], distributed antenna systems [34], and better estimation for Reconfigurable Intelligent Surface (RIS) configuration [35].

ACKNOWLEDGEMENT

This work has been supported by the Spanish Government (grant PID2020-112545RB-C52, MICIU/AEI/10.13039/501100011033), AtlanTTic Research Center and ERDF.

REFERENCES

[1] Schwarz, R., "WLAN at 60 GHz, a technology introduction," https://scdn.rohde-schwarz.com/ur/pws/dl downloads/dl application/application notes/1ma220/1MA220 3e WLAN 11ad WP.pdf, 2017.

[2] Alejos, A. V., M. G. Sanchez, and I. Cuinas, "Measurement and analysis of propagation mechanisms at 40 GHz: Viability of site shielding forced by obstacles," *IEEE Transactions on Vehicular Technology*, Vol. 57, No. 6, 3369–3380, Nov. 2008.

[3] Cuiñas, I. and M. G. Sánchez, "Permittivity and conductivity measurements of building materials at 5.8 GHz and 41.5 GHz," *Wireless Personal Communications*, Vol. 20, No. 1, 93–100, 2002.

[4] Cuiñas, I., J.-P. Pugliese, A. Hammoudeh, and M. G. Sánchez, "Frequency dependence of dielectric constant of construction materials in microwave and millimeter-wave bands," *Microwave and Optical Technology Letters*, Vol. 30, No. 2, 123–124, 2001.

[5] Leonor, N. R., R. F. S. Caldeirinha, T. R. Fernandes, D. Ferreira, and M. G. Sánchez, "A 2D ray-tracing based model for micro- and millimeter-wave propagation through vegetation," *IEEE Transactions on Antennas and Propagation*, Vol. 62, No. 12, 6443–6453, Dec. 2014.

[6] Alejos, A. V., L. Pereira, M. G. Sanchez, and M. Dawood, "Development of 3D human tissues phantoms for analysis of frequency dispersion and human body interaction at 60 GHz," in *2015 USNC-URSI Radio Science Meeting (Joint with AP-S Symposium)*, 368–368, Vancouver, BC, Canada, 2015.

[7] MacCartney, G. R., T. S. Rappaport, and S. Rangan, "Rapid fading due to human blockage in pedestrian crowds at 5G millimeter-wave frequencies," in *GLOBECOM 2017 — 2017 IEEE Global Communications Conference*, 1–7, Singapore, 2017.

[8] Senic, J., A. Bhardwaj, C. Gentile, D. Caudill, C. Lai, D. Senic, S. Y. Jun, J. Chuang, J. Wang, A. Bodi, R. Caromi, and N. Golmie, "Challenges for 5G and beyond," in *2022 16th European Conference on Antennas and Propagation (EuCAP)*, 1–5, Madrid, Spain, 2022.

[9] Alyosef, A., S. Rizou, Z. D. Zaharis, P. I. Lazaridis, A. M. Nor, O. Fratu, S. Halunga, T. V. Yioultsis, and N. V. Kantartzis, "A survey on the effects of human blockage on the performance of mmWave communication systems," in *2022 IEEE International Black Sea Conference on Communications and Networking (BlackSeaCom)*, 249–253, Sofia, Bulgaria, 2022.

[10] Testolina, P., M. Lecci, A. Traspadini, and M. Zorzi, "An open framework to model diffraction by dynamic blockers in millimeter wave simulations," in *2022 20th Mediterranean Communication and Computer Networking Conference (MedComNet)*, 9–17, Pafos, Cyprus, 2022.

[11] Salous, S., Y. He, J. Hu, A. Al-Jzari, and S. Kodra, "Human blockage measurements using multiband CW sounder," in *2025 19th European Conference on Antennas and Propagation (EuCAP)*, 1–5, Stockholm, Sweden, 2025.

[12] ITU-R, "Propagation by diffraction," Recommendation ITU-R P.526-15, Oct. 2019.

[13] Anglès-Vázquez, A., E. Carreño, and L. S. Ahumada, "Modeling the effect of pedestrian traffic in 60-GHz wireless links," *IEEE Antennas and Wireless Propagation Letters*, Vol. 16, 1927–1931, 2017.

[14] Ahumada Fierro, L., E. C. Maggi, A. A. Vazquez, and D. Schkolnik, "Empirical results for human-induced shadowing events for indoor 60 GHz wireless links," *IEEE Access*, Vol. 8, 44 522–44 533, 2020.

[15] Jacob, M., S. Priebe, A. Maltsev, A. Lomayev, V. Erceg, and T. Kürner, "A ray tracing based stochastic human blockage model for the IEEE 802.11 ad 60 GHz channel model," in *Proceedings of the 5th European Conference on Antennas and Propagation (EUCAP)*, 3084–3088, Rome, Italy, 2011.

[16] Zhang, P., P. Kyösti, M. Bengtson, V. Hovinen, K. Nevala, J. Kokkoniemi, and A. Pärssinen, "Measurement-based characterization of D-band human body shadowing," in *2023 17th European Conference on Antennas and Propagation (EuCAP)*, 1–5, Florence, Italy, 2023.

[17] MacCartney, G. R., S. Deng, S. Sun, and T. S. Rappaport, "Millimeter-wave human blockage at 73 GHz with a simple double knife-edge diffraction model and extension for directional antennas," in *2016 IEEE 84th Vehicular Technology Conference (VTC-Fall)*, 1–6, Montreal, QC, Canada, 2016.

[18] Kunisch, J. and J. Pamp, "Ultra-wideband double vertical knife-edge model for obstruction of a ray by a person," in *2008 IEEE International Conference on Ultra-Wideband*, Vol. 2, 17–20, Hannover, Germany, 2008.

[19] Tran, N., T. Imai, and Y. Okumura, "Study on characteristics of human body shadowing in high frequency bands: Radio wave propagation technology for future radio access and mobile optical networks," in *2014 IEEE 80th Vehicular Technology Conference (VTC2014-Fall)*, 1–5, Vancouver, BC, Canada, 2014.

[20] Mukherjee, S., G. Skidmore, T. Chawla, A. Bhardwaj, C. Gentile, and J. Senic, "Scalable modeling of human blockage at millimeter-wave: A comparative analysis of knife-edge diffraction, the uniform theory of diffraction, and physical optics against 60 GHz channel measurements," *IEEE Access*, Vol. 10, 133 643–133 654, 2022.

[21] Bhardwaj, A., D. Caudill, C. Gentile, J. Chuang, J. Senic, and D. G. Michelson, "Geometrical-empirical channel propagation model for human presence at 60 GHz," *IEEE Access*, Vol. 9, 38 467–38 478, 2021.

[22] Galeote-Cazorla, J. E., A. Ramírez-Arroyo, S. Moreno-Rodríguez, J.-M. Molina-García-Pardo, M.-T. Martinez-Inglés, P. Padilla, and J. F. Valenzuela-Valdés, "A study on W-band frequency attenuation in the presence of human blockage," in *2024 18th European Conference on Antennas and Propagation (EuCAP)*, 1–5, Glasgow, United Kingdom, 2024.

[23] Rappaport, T. S., G. R. MacCartney, S. Sun, H. Yan, and S. Deng, "Small-scale, local area, and transitional millimeter wave propagation for 5G communications," *IEEE Transactions on Antennas and Propagation*, Vol. 65, No. 12, 6474–6490, Dec. 2017.

[24] Topal, O. A., M. Ozger, D. Schupke, E. Björnson, and C. Cavdar, "mmWave communications for indoor dense spaces: Ray-tracing based channel characterization and performance comparison," in *ICC 2022 — IEEE International Conference on Communications*, 516–521, Seoul, Korea, 2022.

[25] Doeker, T., M. Eggers, C. E. Reinhardt, D. M. Mittleman, and T. Kürner, "Human motion sensing through blockage and reflection measurements at 60 GHz and 300 GHz," *IEEE Access*, Vol. 13, 97 997–98 005, 2025.

[26] Plouhinec, E. and B. Uguen, "Knife-edge diffraction models for human body shadowing prediction," in *2022 IEEE-APS Topical Conference on Antennas and Propagation in Wireless Communications (APWC)*, 36–41, Cape Town, South Africa, 2022.

[27] Jacob, M., C. Mbianke, and T. Kürner, "A dynamic 60 GHz radio channel model for system level simulations with MAC protocols for IEEE 802.11ad," in *IEEE International Symposium on Consumer Electronics (ISCE 2010)*, 1–5, Braunschweig, Germany, 2010.

[28] IEEE, "IEEE Standard on Transitions, Pulses, and Related Waveforms," 1–60, IEEE Std 181-2003, 2003.

[29] Parsons, J. D., *The Mobile Radio Propagation Channel*, 2nd ed., John Wiley & Sons, Inc., 2001.

[30] Shepherd, N. H., "Radio wave loss deviation and shadow loss at 900 MHz," *IEEE Transactions on Vehicular Technology*, Vol. 26, No. 4, 309–313, Nov. 1977.

[31] Sagias, N. C., G. K. Karagiannidis, P. S. Bithas, and P. T. Mathiopoulos, "On the correlated weibull fading model and its applications," in *2005 IEEE 62nd Vehicular Technology Conference*, 2149–2153, Dallas, TX, USA, 2005.

[32] Jeba, H. A., A. Gaydamaka, and D. Moltchanov, "Distinguishing micromobility and blockage in 6G sub-THz systems: A machine learning approach," *IEEE Open Journal of the Communications Society*, Vol. 6, 7810–7822, 2025.

[33] Zhinuk, F., A. Gaydamaka, D. Moltchanov, and Y. Koucheryavy, "Spectral-based proactive blockage detection for sub-THz communications," *IEEE Communications Letters*, Vol. 28, No. 7, 1703–1707, Jul. 2024.

[34] Moerman, A., O. Caytan, H. Rogier, and S. Lemey, "Millimeter-wave distributed antenna systems for interactive virtual reality: Reducing blockage and exposure and enhancing robustness with (air-filled) substrate-integrated waveguide antennas. [Bioelectromagnetics]," *IEEE Antennas and Propagation Magazine*, Vol. 67, No. 4, 67–78, Aug. 2025.

[35] Neha, B. S., N. S. Rai, K. V. Shilpa, *et al.*, "Human blockage modelling in mmWave link," in *2025 3rd International Conference on Smart Systems for Applications in Electrical Sciences (ICSSES)*, 1–6, Tumakuru, India, 2025.